Model reduction strategies enable computational analysis of controlled drug release from cardiovascular stents

D Angelo, C.; Zunino, P.; Porpora, A.; Morlacchi, S.; Migliavacca, F.

Model reduction strategies enable computational analysis of controlled drug release from cardiovascular stents. *

Carlo D'Angelo, Paolo Zunino, Azzurra Porpora,
Stefano Morlacchi, Francesco Migliavacca

November 23, 2011

MOX - Dipartimento di Matematica "F. Brioschi"
Politecnico di Milano
piazza Leonardo da Vinci 32, 20133 Milano, Italy

Keywords: mass transfer, multiscale modeling, computational analysis, biomedical applications

Abstract

Medicated cardiovascular stents, also called drug eluting stents (DES) represent a relevant application of controlled drug release mechanisms. Modeling of drug release from DES also represents a challenging problem for theoretical and computational analysis. In particular, the study of drug release may require to address models with singular behavior, arising for instance in the analysis of drug release in the small diffusion regime. Moreover, the application to realistic stent configurations requires to account for complex designs of the device. To efficiently obtain satisfactory simulations of DES we rely on a multiscale strategy, involving lumped parameter models (0D) to account for drug release, one dimensional models (1D) to efficiently handle complex stent patterns and fully three-dimensional models (3D) for drug transfer in the artery, including the lumen and the arterial wall. The application of these advanced mathematical models makes it possible to perform a computational analysis of the fluid dynamics and drug release for a medicated stent implanted into a coronary bifurcation, a treatment where clinical complications still have to be fully understood.

1

1 Introduction and motivations

The main limiting factor after stenting interventions for coronary artery diseases remains in-stent restenosis, the re-narrowing of a blood vessel after stent implantation, mainly due to inflammatory healing followed by neointimal proliferation [12]. The most popular approach for the prevention of restenosis consists in the use of the drug eluting stent (DES), a medical device able to release antiproliferative drugs with programmed pharmacokinetics into the arterial wall. The stent acts as a source of drug which is transported into and through the arterial wall. The drug may be any biologically active agent that acts on the cell life cycle so that a step in the replication cascade is inhibited, according to the drug nature [20]. Computational studies on drug elution from stents have been shown to be a very promising tool for the device optimization and have provided insights into the pharmacokinetics of the drug delivered via DES [21, 36, 1]. Most of the studies rely on simplified geometries of stented arteries; only recently some efforts have been devoted to realistic geometries [22, 27, 35].

Besides being a relevant bioengineering application, modelling of DES also represents a challenging problem from the mathematical and computational standpoint. In particular, modeling of drug release from DES features two main difficulties. Firstly, it requires to couple different models with possible singular behavior, i.e. coupling drug release in the small diffusion regime with mass transport in the arterial wall. Secondly, modern stents feature a complex geometrical configuration of the active surface for drug release (see for instance figure 2). Then, a particular effort must be devoted to set up mathematical models that do not require excessive computational resources for their numerical approximation.

To efficiently obtain satisfactory simulations of DES we rely on a multiscale strategy, involving lumped parameter models (0D) to account for drug release, one dimensional models (1D) to efficiently handle complex stent patterns and fully three-dimensional models (3D) for drug transfer in the artery, including the lumen and the arterial wall.

Starting from early works, [27], the multiscale description of drug release from stents has been continuously developed by the authors, by first coupling lumped models for drug release based on pure diffusion, [34], with advection, diffusion, reaction equations for drug pharmacokinetics in the artery, [32, 13]. Recently, the drug release formula has been extended in [2] to a more realistic case combining drug dissolution and diffusion, which has been a well accepted model for drug release for more than fifty years, see for instance [18, 19, 5] for specific contributions, or [26] for a general overview. The main limitation of this model consists in the description of the stent as a three dimensional structure, because at the numerical approximation level this makes it difficult to build up a computational mesh. As shown in [35], a fully 3D model of a single stent cell is achievable, but the extension to multiple cells still represents a computational challenge that cannot be handled with standard computational resources. The

main purpose of this work is to combine the modeling of drug release in the artery with a one dimensional description of the stent structure, inspired by the immersed boundary method and thoroughly developed in [8]. The main advantage of this technique consists in the fact that the geometrical description of the stent does not need to conform with the computational mesh for the artery, remarkably simplifying the steps needed to perform a computational analysis of realistic stents deployed in arterial bifurcations.

To pursue these objectives, we first introduce in section 2 a fully 3D model for drug release from DES to arteries. Then, we present in section 3 an extension of the lumped drug release model addressed in [2] and we discuss the model accuracy with the help of numerical simulation. In section 4 we set up the immersed boundary method for mass transfer on the basis of [8] and we make it specific for drug release by coupling it with the lumped parameter model of section 3. Finally, in section 5, we apply the resulting multi-scale model to the computational analysis of drug release from a realistic DES implanted into a coronary artery bifurcation.

2   Problem set up

The objective of this section is to describe the coupling of drug dissolution and release from medicated stents with drug diffusion and transport in arteries. We introduce a domain $\Omega_c \subset \mathbb{R}^3$ corresponding to the thin substrate surrounding the stent and releasing drug. Moreover, let Γ_s be the interface between Ω_c and the artery, including the lumen and the arterial wall. We assume that the drug release is controlled by drug dissolution and diffusion. To the best of our knowledge, the most recent description and analysis of such phenomena is provided by Frenning in [14, 15]. It consist of a two phase model (solid and dissolved drug) for drug dissolution and diffusion accounting for a finite dissolution rate. In particular, we refer here to the simple case [14] where dissolved drug does not chemically interact with the substrate.

Let $\hat{s}, \hat{c}$ be respectively the concentration of the solid and dissolved drug in the coating, according to the so called Noyes-Whitney formula, see [26], it is possible to quantify the dissolution rate of the solid drug, denoted by $k_d(\hat{s})$ as follows,

$$\frac{k_d(\hat{s})}{\bar{s}} = K \left(\frac{\hat{s}^+}{\bar{s}} \right)^{\frac{2}{3}} \left(\frac{c_s - \hat{c}}{\bar{s}} \right)$$

where $\bar{s}$ is a reference concentration that is often chosen equal to c_s, the saturation level of dissolved drug in water, $K > 0$ is the dissolution constant and $f^+ = \frac{1}{2}(|f| + f)$ denotes the positive part of a function f. As a result of that, denoting with $c = \hat{c}/c_s$, $s = \hat{s}/c_s$, respectively, the nondimensional concentration of the dissolved and solid drug with respect to c_s, with t and $\mathbf{x}$ being the time and space coordinates, the diffusion/dissolution model for drug release reads as

follows,

$$
\begin{cases}
\partial_t c - \nabla \cdot (D_c \nabla c) = K(s^+)^{2/3}(1-c) & \text{in } \Omega_c \times \mathbb{R}^+ \\[2mm]
\partial_t s = -K(s^+)^{2/3}(1-c) & \text{in } \Omega_c \times \mathbb{R}^+ \\[2mm]
s = s_0, \quad c = 0, & \text{in } \Omega_c \times \{t = 0\}
\end{cases}
\tag{1}
$$

complemented with suitable boundary conditions to be addressed later on. In equation (1) $D_c > 0$ is the diffusion coefficient, s_0 is a non-negative function describing the (possibly non-uniform) initial solid drug loading.

For the modeling of the artery we consider a computational domain Ω_a, given by a truncated portion of an artery including both the lumen and the arterial wall, i.e. $\Omega_a = \Omega_w \cup \Omega_l$ where Ω_w represents the arterial wall and Ω_l is the lumen. The boundary $\partial \Omega_a$ can be split into Γ_{adv}, the interface with the outer wall tissue called *adventitia*, Γ_{cut}, the artificial sections where the artery has been truncated from the entire vascular system and $\Gamma_s = \partial \Omega_a \cap \partial \Omega_c$ is the interface with the coating. We denote by $\mathbf{n}_a$ and $\mathbf{n}$ the unit normal vectors associated with Ω_a and Γ_s, respectively. We refer to figure 1 for a schematic illustration of domains and boundaries. We assume that $\mathbf{n}$ is oriented from the stent coating towards the artery, but the arbitrariness of $\mathbf{n}$ will not influence the model setup.
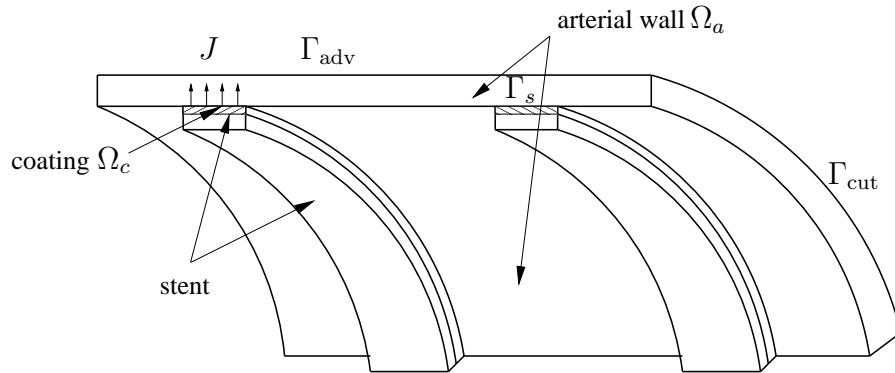

Figure 1: A sketch of two single stent wires laying on the arterial wall, with indication of domains and boundaries for problems (1), (3).

To analyze the distribution of the drug in the artery, we denote by $a(t, \mathbf{x})$ the drug concentration in the artery, which can be split as $a_l(t, \mathbf{x})$ and $a_w(t, \mathbf{x})$ for the lumen and the wall respectively. According to [25, 32], we observe that the drug released into the arterial wall can assume two different states: a state where the drug is dissolved into the plasma permeating the interstices between cells and a state where the drug binds to specific sites of the tissue extracellular matrix. Let us denote by $b_w(t, \mathbf{x})$ the density of the free binding sites, with $b_{w,0}(\mathbf{x}) = b_w(t = 0, \mathbf{x})$ their initial density and with $d_w(t, \mathbf{x})$ the concentration

4

of the drug attached to the extracellular matrix. We assume that the drug in the state d_w can no longer diffuse or be transported by plasma. By virtue of the mass conservation principle, we immediately get $d_w(t, \mathbf{x}) = b_{w,0}(\mathbf{x}) - b_w(t, \mathbf{x})$. The ligand/receptor interaction between the dissolved drug and the free binding sites is represented by the following equation:

$$a_w + b_w \overset{k_{\mathrm{on}}}{\to} d_w, \quad d_w \overset{k_{\mathrm{off}}}{\to} a_w + b_w \quad \text{in } \Omega_w \qquad (2)$$

where k_{on}, k_{off} are the association and dissociation constants. Due to the mass action law, the previous relations state that the rate of change of d_w is equal to $k_{\mathrm{on}} a_w b_w + k_{\mathrm{off}}(b_w - b_{w,0})$. As regards the lumen, there is no chemical interaction between drug and blood flowing into the artery. Then, we set $b_{l,0} = 0$ and by consequence of (2) we get $b_l(t, \mathbf{x}) = d_l(t, \mathbf{x}) = 0$ for any $\mathbf{x} \in \Omega_l$ and $t > 0$. In conclusion, the transport of drug into the artery can be modeled by means of the following equations:

$$\begin{cases} \partial_t a - \nabla \cdot (D_a \nabla a) + \mathbf{u} \cdot \nabla a + k_{\mathrm{on}} ab + k_{\mathrm{off}}(b - b_0) = 0 & \text{in } \Omega_a \times \mathbb{R}^+ \\[2mm] \partial_t b + k_{\mathrm{on}} ab + k_{\mathrm{off}}(b - b_0) = 0 & \text{in } \Omega_a \times \mathbb{R}^+ \\[2mm] a = a_0(\mathbf{x}), \quad b = b_0(\mathbf{x}) & \text{in } \Omega_a \times \{t = 0\} \\[2mm] a = 0 & \text{on } \Gamma_{adv} \times \mathbb{R}^+ \\[2mm] \nabla a \cdot \mathbf{n}_a = 0 & \text{on } \Gamma_{cut} \times \mathbb{R}^+ \end{cases} \qquad (3)$$

where D_a is the diffusivity of the drug into the arterial tissue or into the blood and $\mathbf{u}$ is the velocity field describing the filtration of the plasma inside the wall or the blood flow in the lumen. A suitable model that governs $\mathbf{u}$ will be addressed later on. Concerning boundary conditions of (3), we observe that the adventitia is perfused by micro-vasculature. Thus, drug reaching this boundary is quickly washed out. A simple model to account for this effect is given by the perfect sink condition on Γ_{adv}. We also assume that drug concentration profiles are unperturbed along Γ_{cut}, if the artificial cuts are located far enough from the drug release source Γ_s.

The model (1), (3) becomes solvable provided that some transmission conditions between Ω_c and Ω_a are defined,

$$c = a, \quad D_a \nabla a \cdot \mathbf{n} = D_c \nabla c \cdot \mathbf{n} \quad \text{on } \Gamma_s \times \mathbb{R}^+. \qquad (4)$$

For the numerical discretization of problem (1),(3),(4) we aim to apply a finite difference scheme in time and a finite element method for the space dependence. This is a strong limitation for the simulation with our model where Ω_c may be 7 μm thin, while Ω_a is comparable to a cylinder 5 mm wide and 20 mm long with a wall thickness of 0.75 mm. A further difficulty, also illustrated by figure 2,

consists in the fact that new generation stents can assume very complex designs. The forthcoming set up of a multi-scale method is mandatory to override these obstacles.

Figure 2: An illustration of a realistic cardiovascular stent implanted into an arterial bifurcation. The stent is depicted by means of its centerline. The length of the visualized portion of artery is about 2 centimeters, while the inner and outer reference diameters are equal to 2.78 and 4.58 millimeters respectively, [16].

3   A lumped model for the release rate

The coating of DES is very thin and to study drug release it can be approximated by a indefinite slab. For this reason, the domain Ω_c becomes a one dimensional interval with space coordinate $x \in (0, L)$, L being the thickness of the stent surface coating. We first address the nondimensional form of equation (1). We select L as reference length, K^{-1} as reference time (being K the dissolution constant in the aforementioned Noyes-Whitney model) and c_s as reference concentration. Then, given $\tau = Kt$, $y = x/L$ the nondimensional time and space

coordinates, respectively, the nondimensional counterpart of (1) reads as follows,

$$
\begin{cases}
\partial_\tau c - \Lambda \partial_{yy} c = (s^+)^{2/3}(1-c) & \text{in } (0,1) \times \mathbb{R}^+ \\[2mm]
\partial_\tau s = -(s^+)^{2/3}(1-c) & \text{in } (0,1) \times \mathbb{R}^+ \\[2mm]
\partial_y c = 0 & \text{on } \{0\} \times \mathbb{R}^+ \\[2mm]
c = a(\tau) & \text{on } \{1\} \times \mathbb{R}^+ \\[2mm]
s = s_0, \ c = 0, & \text{in } (0,1) \times \{t=0\}
\end{cases}
\tag{5}
$$

where the fundamental characteristic parameter Λ (known as Thiele modulus) is defined as

$$
\Lambda := \frac{D_c}{KL^2}
$$

and $a(\tau)$ is an assigned function that will be later replaced with the drug concentration in the arterial wall, according to (4). For any dissolution based drug release system, it is mandatory to assume $0 \le a(\tau) < 1$; otherwise drug release is prevented by adverse concentration gradients. Furthermore, for the sake of simplicity, we restrict ourselves to the case of uniform initial drug loading: thus $s_0 > 0$ is a constant.

The parameter Λ, controlling the balance between diffusion and reaction, is indeed one of the most significant to determine the behavior of the system. It can be also interpreted as the ratio between the characteristic time of reaction and diffusion, i.e. in the regime of small Λ diffusion is much slower than reaction. A slow release rate is often desirable, because the released drugs can be toxic at high concentrations. This is for instance the case for release devices such as patches, implantable tablets, drug eluting stents. For this reason, the small diffusion regime is the most interesting from the point of view of applications.

The initial state of the system, namely s_0, is another significant parameter. If the initial drug load is larger than the saturation level of dissolved drug, taken here as unit reference concentration, we say that the substrate has been charged with a saturated loading. In the opposite case, we talk about unsaturated loading.

The initial and boundary conditions of (5) are chosen such as to model the following physical situation. We assume that at the initial time all the drug is loaded in the solid phase, and thus $c(x,0) = 0$ for all x. The extreme points of the substrate respectively represent an inert boundary at $x = 0$, where no drug is released, while at $x = 1$ the external medium maintains the concentration level $a(\tau)$. Indeed, with respect to the analysis performed in [2], we consider here a slightly more general case, because $a(\tau)$ is here a given function that will be later replaced by $a(t, \mathbf{x})$ on Γ_s. However, the forthcoming analysis relies on a quasi-steady approximation for $a(\tau)$. More precisely, we formulate the following assumptions that will be later justified by means of model (3).

Assumption 3.1 *The external drug concentration $a(\tau)$ is such that:*

$$\max_\tau |\partial_\tau a(\tau)| = |\partial_\tau a(\tau = 0)|;$$

increments of $a(\tau)$ are small, i.e. $|a(\tau) - a(0)| \ll \tau$;

As a result of 3.1 we easily conclude that $a(\tau)$ is *quasi-steady* because,

$$|\partial_\tau a(\tau)| \leq |\partial_\tau a(\tau = 0)| \simeq \tau^{-1} |(a(\tau) - a(0))| \simeq 0. \tag{6}$$

For the aforementioned reasons, we restrict our analysis to the small diffusion regime, $\Lambda \ll 1$, with saturated loading, $s_0 > 1$ and we briefly summarize the behavior of (5) in this case. In particular, we address in figure 3 the numerical approximation of its solutions, in a case with mildly stiff coefficients, i.e. $\Lambda = 10^{-2}$, $s_0 = 3$, $a(\tau) = 0.5$. Different coefficients, corresponding to the application of drug eluting stents will be discussed in section 5.

Under these conditions, the dynamics of the system can be split into two phases, the former dominated by reaction and the latter by diffusion. The evolution starts with a sudden decrease of solid drug concentration, that jumps from the initial state $s = s_0$ to $s \simeq s_0 - 1$ and $c \simeq 1$, where the difference $1 - c$ is positive but almost vanishing, see figure 3 (top). Without the influence of the external boundary, the state variables s, c would converge to $s = s_0 - 1, c = 1$ with $c(\tau, x) < 1$ and $s(\tau, x) > s_0 - 1$ for any $x \in (0, 1)$. In this phase, the concentration jump $1 - c$ is almost completely absorbed, i.e. $c \simeq 1$, except that in the neighborhood of the external boundary, where the drug concentration is fixed to $c = a(\tau) < 1$. It is shown in [2] that the characteristic time of this phase is proportional to $s_0^{1/3}$, which is very small with respect to the characteristic time needed to release the entire drug load.

Because of the interplay between the diffusion operator and the Dirichlet boundary condition $c(\tau, 1) = a(\tau)$, the state $s = s_0 - 1, c = 1$ is perturbed, and the system shifts to a stable equilibrium $s = 0, c = a(\tau)$. This is the second transition phase for the saturated loading problem and it is shown in figure 3 (bottom). Due to the boundary condition $c = a(\tau)$, the highest drug concentration jump with respect to the saturation level is now located at $x = 1$, and starting from this point a propagating front for the solid drug concentration s moves towards the inner part of the interval $(0, 1)$. In doing so, it leaves behind a region in which $s = 0$, where c obeys a simple homogeneous diffusion equation.

For such system configuration, we aim to study how the release rate varies during the evolution of the moving front. We denote by $Y(\tau) \in (0, 1)$ the interface that discriminates between the region where $s(y, \tau) > 0$ and $s(y, \tau) = 0$. The propagating front subdivides the interval $(0, 1)$ into three subregions; the internal region $(0, Y(\tau) - \delta)$ where for any point y the solid drug concentration $s(y, \tau) \simeq s_0 - 1$, the intermediate layer $(Y(\tau) - \delta, Y(\tau))$ whose thickness $\delta = O(\sqrt{\Lambda})$ when $\Lambda \to 0^+$ remains constant along the dissolution process, and the depleted one that is $(Y(\tau), 1)$ where the solid drug has dissolved into free drug,

i.e. $s(y, \tau) = 0$. Since the propagating front moves from the external boundary $y = 1$ inward to the domain, we assert that $\dot{Y}(\tau) < 0$. We notice that the evolution of the system in the second phase is much slower than in the first one. Indeed, the state $s \simeq s_0 - 1$ and $c \simeq 1$ is reached for $\tau \simeq 2$ (nondimensional time units), while the second transition requires $\tau \simeq 300$ to approach the final state $s \simeq 0$, $c \simeq a$.

$s(t, y)$ $\qquad\qquad\qquad\qquad\qquad$ $c(t, y)$

$s_0 = 3$, $t \in [0, 2]$ time evolves from top to bottom for s and inversely for c

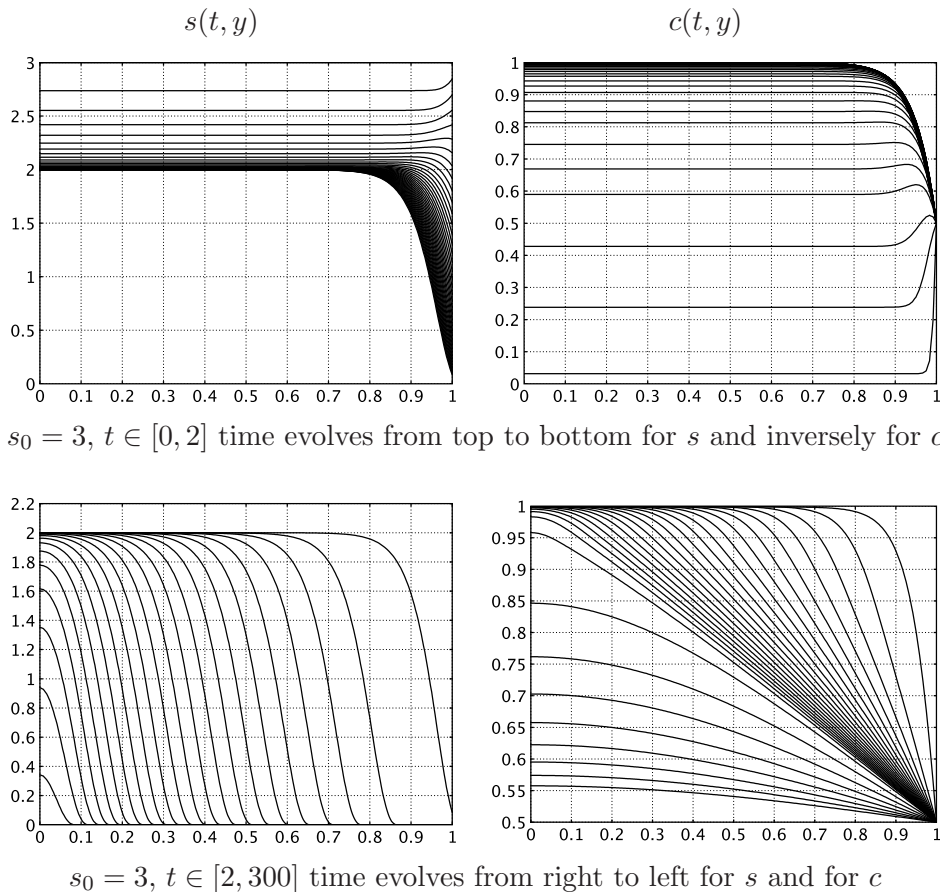$s_0 = 3$, $t \in [2, 300]$ time evolves from right to left for s and for c

Figure 3: Numerical solutions of problem (5), plotted with respect to the nondimensional space coordinate $y \in (0, 1)$ and for different time scales.

Due to (6) it is possible to mimic the analysis preformed in [2] in order to derive an analytic expression for the drug release rate from the stent coating. For the sake of clarity, we recall here the main steps of the derivation addressed in [2], Section 4.3. On the basis of the aforementioned observations, we seek solutions of (5) that might be expanded in terms of the parameter Λ, where the

first terms of the expansion are given by

$$\tilde{s}(y,\tau) = \begin{cases} 0 & \text{if } y > Y(\tau)) \\ \varsigma\left(\dfrac{y - Y(\tau)}{\sqrt{\Lambda}}\right) & \text{if } Y(\tau) - \delta < y < Y(\tau) \\ s_0 - 1 & \text{if } y < Y(\tau) - \delta, \end{cases} \tag{7}$$

$$\tilde{c}(y,\tau) = \begin{cases} a(\tau) + c_{\text{diff}}(y,\tau) & \text{if } y > Y(\tau) \\ 1 & \text{if } y < Y(\tau), \end{cases}$$

where ς and c_{diff} are functions to be determined. In particular, c_{diff} can be interpreted as the dissolved drug concentration in the substrate that is superposed to the bulk value $a(\tau)$, determined by the external conditions. Solutions (7) represent the qualitative behavior of the system in the case of saturated drug loading and long time scales, as illustrated in figure 3 (bottom). Replacing $(7)_b$ for $y > Y(\tau)$ in (5) and exploiting (6) we obtain the diffusion problem

$$\partial_\tau c_{\text{diff}} - \Lambda \partial_{yy} c_{\text{diff}} = 0, \ c_{\text{diff}}(1,\tau) = 0, \ c_{\text{diff}}(Y(\tau),\tau) = 1 - a(\tau) \tag{8}$$

for which we seek self-similar solutions of the form

$$c_{\text{diff}}(y,\tau) = \big(1 - a(\tau)\big)\gamma\left(\frac{1 - y}{1 - Y(\tau)}\right), \ \gamma(y = 1) = 0, \ \gamma(y = Y(\tau)) = 1 \tag{9}$$

where γ is a (positive) function to be determined. We observe that applying a change of variables from y to $z = (1 - y)/(1 - Y)$ and replacing (9) in (8) the following boundary value problem is obtained for $\gamma(z)$,

$$\Lambda\gamma'' - \dot{Y}(1 - Y)z\gamma' = 0, \ \gamma(0) = 0, \ \gamma(1) = 1 \tag{10}$$

Exploiting $(1 - Y) > 0$ and $\dot{Y} < 0$, we set $\Gamma^2 := -\dot{Y}(1 - Y)/(2\Lambda)$. As a result of that (10) can be rewritten as,

$$\gamma'' + 2\Gamma^2 z\gamma' = 0, \ \gamma(0) = 0, \ \gamma(1) = 1$$

which admits the following family of solutions

$$\gamma(z) = \frac{\text{erf}(\Gamma z)}{\text{erf}(\Gamma)} \tag{11}$$

where Γ will be determined from $\dot{Y}$, i.e. the speed of propagation at which the front of the solid drug $s(\tau,y)$ evolves towards $y = 0$. As performed in the seminal work by Higuchi, [18], $\dot{Y}$ can be estimated by a simple mass-balance argument. Indeed, the amount of drug stored in the whole system at any time τ is given by

$$Q(\tau) = \left[(s_0 - 1)(Y - \delta) + \int_{Y-\delta}^{Y} \varsigma \, dy\right] + \left[Y + (1 - Y)a + (1 - a)\int_{Y}^{1} \gamma \, dy\right]$$

10

where the terms within the brackets respectively correspond to the amount of drug stored in the solid and in the liquid phase. The time derivative of Q, i.e. $\dot{Q}$, must be balanced by the release rate. Due to (6), the external concentration $a(\tau)$ is assumed to be constant with time. The first integral on the right hand side is also constant. After a change of variables from y to z in the last integral such that $\int_Y^1 \gamma \, dy = (1-Y) \int_0^1 \gamma(z) \, dz$, where $\int_0^1 \gamma(z) \, dz$ is constant with respect to τ, we obtain

$$\dot{Q} = s_0 \dot{Y} - a\dot{Y} - (1-a)\dot{Y} \int_0^1 \gamma(z) \, dz.$$

The release rate from the stent coating is defined as $\Upsilon(\tau) := -\Lambda \partial_y c(\tau, y = 1)$ that, due to (9), can be rewritten as

$$\Upsilon(\tau) = \frac{\Lambda(1-a)\gamma'(z=0)}{1-Y} \tag{12}$$

and according to the mass conservation principle $\dot{Q} = \Upsilon(\tau)$ leads to

$$\left(s_0 - a - (1-a) \int_0^1 \gamma(z) \, dz \right) \dot{Y} = \frac{\Lambda(1-a)\gamma'(0)}{1-Y}$$

that can be manipulated as follows

$$\Gamma^2 = \frac{(1-a)\gamma'(0)}{2\left(s_0 - a - (1-a) \int_0^1 \gamma(z) \, dz \right)}. \tag{13}$$

Equation (13) represents a compatibility condition that allows us to implicitly determine Γ. Indeed, by replacing (11) in (13) we obtain

$$\frac{\exp(-\Gamma^2)}{\sqrt{\pi}\Gamma \mathrm{erf}(\Gamma)} = \frac{s_0 - 1}{1 - a} \tag{14}$$

whose solution can be approximated by means of a numerical algorithm. Then, assuming that Γ is known and due to the expression $\Gamma^2 = -\dot{Y}(1-Y)/(2\Lambda)$, the velocity of propagation of the dissolution front satisfies the Cauchy problem,

$$\dot{Y}(\tau) = -\frac{2\Lambda\Gamma^2}{1-Y(\tau)}, \quad Y(\tau = 0) = 1$$

which admits the solution $Y(\tau) = 1 - 2\sqrt{\Lambda\Gamma^2\tau}$ allowing us to compute the time at which the front touches the point $y = 0$, i.e. $\mathcal{T} = \left(4\Lambda\Gamma^2 \right)^{-1}$ in nondimensional variables. We notice that for $\tau > \mathcal{T}$ all the solid drug has dissolved into the dispersed state and by consequence most of the drug has been released (as it will be verified in the forthcoming section). Furthermore, the present model is no longer valid, because the release rate will be then regulated by the pure diffusion problem,

$$\partial_\tau c - \Lambda \partial_{yy} c = 0, \quad \text{with} \quad c(1, \tau) = a(\tau) \quad \text{and} \quad \partial_y c(0, \tau) = 0.$$

In conclusion, replacing the expression of $Y(\tau)$ in (12) we obtain an explicit expression for the release rate

$$\Upsilon(\tau) = -\big(1 - a(\tau)\big)\big(\mathrm{erf}(\Gamma)\big)^{-1}\sqrt{\frac{\Lambda}{\pi\tau}}$$

that can be translated into dimensional form for time and space, but still nondimensional for concentrations,

$$J(t) = -\big(1 - a(t)\big)\big(\mathrm{erf}(\Gamma)\big)^{-1}\sqrt{\frac{D_c}{\pi t}} \qquad (15)$$

that is valid until the final time $T = L^2/(4D_c\Gamma^2)$.

We observe that equation (15) admits a straightforward physical interpretation in analogy with Fick's law of diffusion. Indeed, $\big(1 - a(t)\big)$ corresponds to a discrete drug concentration gradient through the coating, where 1 is the bulk concentration and $a(t)$ is the external concentration, while the term $P(t) := \sqrt{(D_c)/\mathrm{erf}^2(\Gamma)(\pi t)}$ can be interpreted as a permeability coefficient that modulates the intensity of the gradient.

The efficacy of (15) for predicting the release rate will be later verified by means of a comparison with the classical Higuchi model [18, 19] and also with the numerical solution of problem (5) in order to verify the validity of (15) in presence of an external concentration $a(\tau)$ satisfying assumption 3.1.

3.1 Preliminary validation of the lumped drug release model

The release rate expression (15) is first compared with the Higuchi's model, see [18, 19, 26], which under a derivation similar to the one of section 3 but based on stronger assumptions, obtains an analogous formula. Comparing the Higuchi's formula for drug release rate, $J^H(t)$, with $J(t)$ we obtain

$$J^H(t) = -\sqrt{\frac{(2s_0 - 1)D_c}{\pi t}}, \quad J(t) = -(1 - a)\big(\mathrm{erf}(\Gamma)\big)^{-1}\sqrt{\frac{D_c}{\pi t}}. \qquad (16)$$

We notice that, although similar to $J^H(t)$, (15) generalizes Higuchi's expression by modulating the release rate with the nonhomogeneous external concentration, term $1 - a(\tau)$, and by differently accounting for the effect of dissolution, term $(\mathrm{erf}(\Gamma))^{-1}$ instead of $\sqrt{(2s_0 - 1)}$. Furthermore, exploiting (14) to rewrite s_0 in terms of a and Γ and replacing this expression in J^H, taking the limit $s_0 \to 1$ or equivalently $\Gamma \to \infty$ we obtain $J/J^H \to (1 - a)$. This shows that, for $a \to 0$ and $s_0 \to 1$ the expressions of J_H and J match. We also compare the relative amount of drug released defined as $q(t)/q_\infty$ where $q(t) := |\Gamma_s| \int_0^T J(t)dt$ is the amount of drug released and $q_\infty = s_0 L |\Gamma_s|$ is the total drug that can be released during an arbitrarily long time (it is also equivalent to the initial charge of the

stent). The comparison with Higuchi's model gives,

$$\frac{q^H(t)}{q_\infty} = (Ls_0|\Gamma_s|)^{-1}\sqrt{4\pi^{-1}(2s_0-1)D_ct},$$

$$\frac{q(t)}{q_\infty} = (Ls_0|\Gamma_s|)^{-1}\big(1-a(\tau)\big)\big(\mathrm{erf}(\Gamma)\big)^{-1}\sqrt{4\pi^{-1}D_ct}.$$

(17)

In figure 4 we report the comparison among (16) and (17) with the parameters $a = 0$, $s_0 = 10$ and $D_c = 10^{-8}$ mm^2/s, which will be more carefully discussed in section 5 for the application of drug eluting stents. For $t < T$ the two expressions closely match. In particular, we observe that $(17)_b$ can be considered slightly more accurate than $(17)_a$ because at time T the relative amount of drug released per unit surface approaches from below the unit value. It is shown in [2] and also confirmed by numerical simulations that at time T the only drug remaining in the coating is in the dissolved phase, c, and it assumes an almost linear profile connecting $c = 1$ at $x = 0$ with $c = a \simeq 0$ at $x = L$. Then, the residual amount of drug resident in the coating can be estimated as $1/(2s_0)$. Thus, if $s_0 = 10$, almost the 95% of drug has been released at time T.
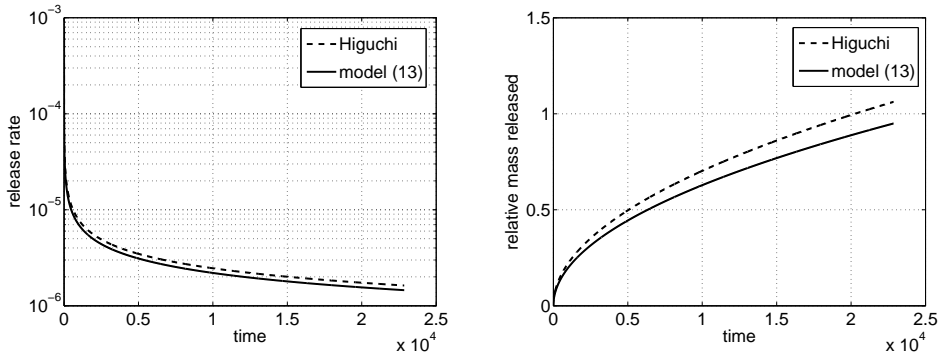

Figure 4: A comparison of fluxes per unit surface (16) (left) and relative amount of drug released (17). The solid line represents the present model, the dashed line depicts Higuchi's formulas.

The validity of (15) for a time dependent external concentration $a(\tau)$ could be investigated by exploiting the numerical approximation of problem (5), performed exploiting Lagrangian finite elements for the space discretization and backward finite difference schemes to advance in time. For further details, we refer to [31, 17]. The main difficulty consists in the efficient solution of the nonlinear system of equations corresponding to the fully discrete scheme. To this aim, we have applied the damped Newton method proposed in [11]. We denote by $c_h(t,x)$, $s_h(t,x)$ the numerical solution of (5) in dimensional coordinates. Accordingly, $J_h(t) = -D_c\partial_x c_h(t, x = L)$ is the release rate computed

13

with the numerical simulations, that will be compared to $J(t)$ in (15). On this basis, we consider several tests for different values of nonhomogeneous Dirichlet datum, $a(\tau)$ in (5), and we fix L, D_c, s_0 to realistic values reported in section 5. We first start from the verification that, when $a(\tau) = 0$, it is true that $J(t) \simeq J_h(t)$. This is indeed verified since the computed relative error, $|J(t) - J_h(t)|/|J_h(t)| \simeq 1\%$. Then, we address the case of nonhomogeneous but constant Dirichlet datum, $a(\tau) = 0.5$ and due to the analysis previously developed, we expect that this case should be equivalent to the homogeneous one, as confirmed by a relative error equivalent to 1% even though $a = 0.5$ cannot be considered to be small. Finally, we perform the comparison for a small, but time dependent value of $a(\tau)$, such as assumption 3.1 is satisfied. More precisely, setting $a(\tau) = 0.0316(\tau + 0.1)^{-\frac{1}{2}}$ such that $a(0) = 0.1$, the relative error between the fluxes is again nearby 1%, which confirms that under assumption 3.1 the expression (15) represents an accurate approximation of the exact release rate. We do not report the corresponding visual comparisons because the curves are almost superimposed in all cases.

4 An immersed boundary method for drug release from thin devices

Immersed boundary methods were first introduced by Peskin [28, 29] to efficiently simulate flow around heart valves and they rely upon the idea of replacing an immersed interface with the related interface conditions by an equivalent forcing term. By using such techniques, we will be able to avoid resolving the complex 3D geometry of the stent; basically we will only need the 1D geometrical description of the centerline Λ_s, as depicted in figure 5. The application of the forthcoming immersed boundary method for modeling stents has two main consequences: on one hand, we neglect the stent in the blood flow model (where it would act as an obstacle); on the other hand, we represent the stent as an immersed boundary in the mass transport model (where it acts as a mass source, releasing drug).

4.1 Model set up

Let Ω be a generic domain and let Γ_s be the portion of *active* surface that is embedded in Ω. For the models presented in section 2, Ω corresponds to the artery Ω_a and Γ_s is the stent surface releasing drug. The mass flux released by Γ_s is denoted by f, that is a mass flux per unit area. From the modeling point of view, if $a(t, \mathbf{x})$ with $\mathbf{x} \in \Gamma_s$ is the drug concentration in the artery, then $f(t, a(t, \mathbf{x}))$ is a pointwise constitutive law for the release rate.

In this work, as in standard immersed boundary methods, we will consider the case in which the action of f is represented as an equivalent source term, F, distributed on the entire domain Ω. More precisely, $F = F(t, a)$ is a *measure*
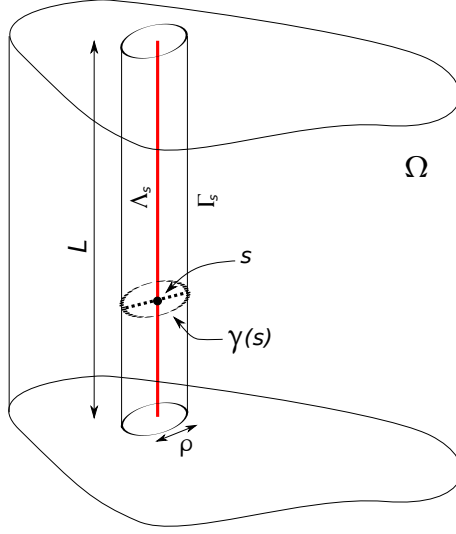
Figure 5: Immersed boundary $\Gamma_s \subset \Omega$ (the actual surface of the stent).

defined by

$$\int_\Omega F(t,a)v = \int_{\Gamma_s} f(t,a)v \quad \forall v \in C(\Omega) \tag{18}$$

where v plays the role of a test function in the variational formulation of problem (3). Hence, we use the notation $F(t,a) = f(t,a)\delta_{\Gamma_s}$ meaning that F is the Dirac measure concentrated on Γ_s, having (time and concentration dependent) density f on Γ_s. Following the lines of [9] (see also [8] for a theoretical study of the resulting mathematical model), we represent such mass flux per unit area by an equivalent mass flux *per unit length*, distributed on the centerline Λ_s of the stent. Assuming that Γ_s has a circular transversal section, with small radius ρ, we approximate the action of F on v in (18) by a similar equivalent one-dimensional formulation based on numerical integration. Referring to figure 5, and using cylindrical coordinates (s,θ) on Γ_s, we have

$$\int_\Omega F(t,a)v = \int_{\Lambda_s} \int_{\gamma(s)} f(t,a(t,s,\rho,\theta))v(s,\rho,\theta)\rho\,\mathrm{d}\theta\mathrm{d}s.$$

Then, applying the (midpoint) rectangle quadrature formula to approximate the integral over the arc $\gamma(s)$ (of radius ρ) given by the intersection of Γ_s with the normal plane to Λ_s at point s, we have, for $g = v, a$,

$$\bar{g}(s) := \frac{1}{|\gamma(s)|} \int_{\gamma(s)} g(s,\rho,\theta)\mathrm{d}\theta = g(s,\rho,\theta = \pi) + O(|\gamma(s)|^3)$$

where $\mathcal{O}(x^3)$ denotes any function such that $lim_{\rho\to\infty}\mathcal{O}(x^3)/x^3 = C > 0$. Due to

the rectangle quadrature formula:

$$\int_\Omega F(t,a)v \simeq \int_{\Lambda_s} |\gamma(s)| f(t, \bar{a}(s)) \bar{v}(s) \mathrm{d}s. \tag{19}$$

The coupling between the immersed boundary model for the stent and the lumped model for drug release is easily achieved by replacing (15) in the definition of $f(t,a)$, more precisely setting

$$f(t,a) := P(t)(1-a), \text{ with } P(t) = \big(\mathrm{erf}(\Gamma)\big)^{-1} \sqrt{\frac{D_c}{\pi t}}.$$

Then, fixing the generic domain Ω to Ω_a and defining,

$$\int_{\Omega_a} F_a(t,a)v := 2\pi\rho P(t) \int_{\Lambda_s} \xi(s)(1 - \bar{a}(s))\bar{v}(s)\mathrm{d}s \tag{20}$$

we obtain a one-dimensional model for drug release from a stent. In equation (20), the function $\xi(s) = |\gamma(s)|/(2\pi\rho)$ with $0 \le \xi(s)$ locally quantifies the fraction of stent surface that is embedded into the artery. By splitting the artery into lumen, Ω_l, and wall, Ω_w, we will later denote by $\xi_l(s)$ and $\xi_w(s)$ respectively, the part of stent surface exposed to one or other sub-domains.

According to (20) equation (3) becomes,

$$\begin{cases} \partial_t a - \nabla \cdot (D_a \nabla a) + \mathbf{u} \cdot \nabla a = F_a(t,a) + \partial_t b & \text{in } \Omega_a \times \mathbb{R}^+ \\ \partial_t b + k_{\mathrm{on}} ab + k_{\mathrm{off}}(b - b_0) = 0 & \text{in } \Omega_a \times \mathbb{R}^+ \end{cases} \tag{21}$$

whilst initial and boundary conditions are as in (3), the coupling conditions (4) are now taken into account by F_a due to the immersed boundary formulation.

4.2 Numerical approximation

For the numerical approximation of the weak counterpart of problem (21) we consider a standard implicit Euler time advancing scheme together with piecewise linear finite element space discretization. For the space approximation we first introduce $\mathcal{T}_h$ being a family of conforming triangulations made of affine simplexes K. We also denote by $\mathcal{F}_h$ the set of all interior faces F of $\mathcal{T}_h$. The corresponding space of linear finite elements is denoted by V_h. It is well known that the standard Galerkin-FEM method is unsatisfactory for singularly perturbed problems such as the advection dominated problem for drug transport in the blood flow. For this reason we employ a continuous interior penalty (CIP) stabilization (see [3, 4]). We denote by $a_h(t)$ the approximation of $a(t,\mathbf{x})$ and with $\mathbf{u}_h$ the approximation of steady blood flow and plasma filtration, obtained exploiting the methods addressed in [10]. The main features of the numerical

approximation method are characterized by the following bilinear form,

$$B_a(a_h(t), \psi_h) = \int_{\Omega_a} D_l \nabla a_h(t) \cdot \nabla \psi_h + \int_{\Omega_a} \mathbf{u}_h \cdot \nabla a_h(t) \psi_h$$

$$+ \int_{\Lambda_s} 2\pi\rho P(t)\xi \bar{a}_h(t)\bar{\psi}_h$$

$$+ \int_{\mathcal{F}_{l,h}} \gamma_{\mathbf{u}} \frac{(h_F)^2}{|\mathbf{u}_h|_F} [\![(\mathbf{u}_h \cdot \nabla)a_h(t)]\!][\![(\mathbf{u}_h \cdot \nabla)\psi_h]\!].$$

The space discretization must be complemented with a time advancing scheme. Let $\Delta t > 0$ be time step, $t_n = n\Delta t$ the n-th time step and $a_h^n \in V_{i,h}$ the numerical approximation of $a(t^n)$. The time advancing scheme reads as follows: *given $a_h^n \in V_h$, find $a_h^{n+1} \in V_h$ such that*

$$\frac{1}{\Delta t} \int_{\Omega_a} a_h^{n+1}\psi_h + B_a(a_h^{n+1}, \psi_h) = \frac{1}{\Delta t} \int_{\Omega_a} a_h^n \psi_h$$

$$+ \int_{\Lambda_s} 2\pi\rho P(t^{n+1})\xi \bar{a}_h^{n+1}\bar{\psi}_h \quad \forall \psi_h \in V_{i,h}. \quad (22)$$

The error analysis of the present scheme can be addressed with the tools provided in [8] and [4].

4.3 A numerical validation of the immersed boundary model

Our modeling technique is *de facto* an immersed boundary method. However, since the immersed boundary is the surface of a thin cylinder, Γ_s, the resulting source terms will behave similarly to Dirac measures concentrated on the centerline Λ_s. In this case, it is known that the solution is singular on Λ_s, [8], and the analysis of the accuracy of our immersed boundary model is particularly important. We address this issue by means of a sequence of numerical tests.

   We consider the following steady model problem. Let be $\Omega = \{(z, r, \theta) \in (0, 1) \times [0, 1) \times [0, 2\pi)\}$ (in cylindrical coordinates) and let $\partial\Omega$ be the disjoint union $\Gamma_D \cup \Gamma_N$, with $\Gamma_D = \{\mathbf{x} \in \partial\Omega : r = 1\}$. We introduce a parametrized line $\Lambda_s \subset \Omega$ and generate the curvilinear cylinder Θ_ρ by sweeping a (small) circle of radius ρ along Λ_s. The resulting external surface Γ_s, with outgoing unit normal vector $\mathbf{n}$, is the immersed boundary. Then, we define the domain $\Omega_\rho := \Omega \backslash \Theta_\rho$, and compare the solutions of the following two problems:

$$\begin{cases} -D\Delta a_\rho = 0 & \text{in } \Omega_\rho, \\ \partial_{\mathbf{n}} a_\rho = P(1 - a_\rho) & \text{on } \Gamma_s, \\ \partial_{\mathbf{n}} a_\rho = 0 & \text{on } \Gamma_N, \\ a_\rho = 0 & \text{on } \Gamma_D, \end{cases} \qquad \begin{cases} -D\Delta a = F(a) & \text{in } \Omega, \\ \\ \partial_{\mathbf{n}} a = 0 & \text{on } \Gamma_N, \\ a = 0 & \text{on } \Gamma_D, \end{cases} \qquad (23)$$

where D is the diffusion coefficient and $F(a) = P(1-a)\delta_{\Gamma_s}$ is defined as in (18).

   At least for ρ small, we expect the immersed boundary solution a to be a good approximation of a_ρ in Ω_ρ. To quantify the accuracy of the immersed
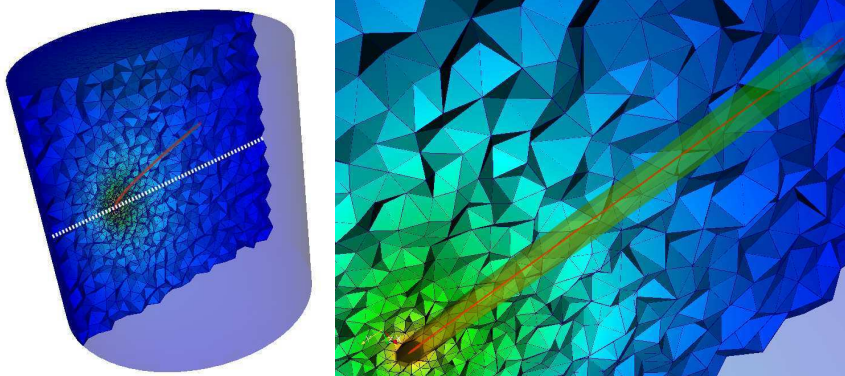
17

Figure 6: On the left: the domain Ω_ρ featuring the thin inclusion Θ_ρ considered in problem (23). The dashed line will be used for sampling solution profiles. On the right: zoom on the line Λ_s (in red), showing the external surface Γ_s of the inclusion Θ_ρ. The domain Ω is precisely $\Omega_\rho \cup \Theta_\rho$.

boundary solution, we perform several computations on different meshes and report the percent relative errors in Ω_ρ in Table 1. In particular, we compute the solution a_ρ on five meshes $\mathcal{T}_h^{(N)}$ (whose element number is denoted by N), covering the whole domain Ω. Then we approximate a_ρ on a sufficiently refined mesh $\mathcal{T}_{\rho,h}^{(N_\rho)}$ of Ω_ρ (whose element number is denoted by N_ρ).

		N				
ρ	N_ρ	53446	97792	121315	455952	844244
$1.25 \cdot 10^{-2}$	629469	(8.3, 49.7)	(6.8, 24.7)	(6.9, 24.4)	(6.9, 24.4)	(6.8, 20.6)
$6.25 \cdot 10^{-3}$	2393248	(5.1, 56.5)	(1.5, 25.5)	(1.5, 25.9)	(1.4, 25.3)	(1.4, 15.4)

Table 1: Mesh invariance tests. Shown are the relative errors $\|a_\rho - a\|/\|a_\rho\|$ (% units) measured in $(L^2(\Omega_\rho), H^1(\Omega_\rho))$ norms, for different values of the element number N_ρ of the mesh on Ω_ρ, of the element number N of elements of the mesh on Ω, and of the radius ρ. The mesh corresponding to $N = N^{(1)}$ was uniform, whilst the other meshes were graded near Λ_s (as shown in Fig. 6).

All computations were done for the nondimensional form of (23), with the characteristic parameter $k = LP/D = 1$, L being the characteristic length of Ω. Due to linearity, we expect relative errors to be independent of k. Errors between the *full* model governing a_ρ and the immersed boundary model governing a represent our *model error*, i.e. the error introduced by the immersed boundary representation of our embedded surface.

The results confirm that the immersed boundary solution, a, is an accurate approximation of the solution a_ρ computed by means of a real internal boundary with transmission conditions, at least in the limit case when the mesh $\mathcal{T}_h^{(N)}$ is
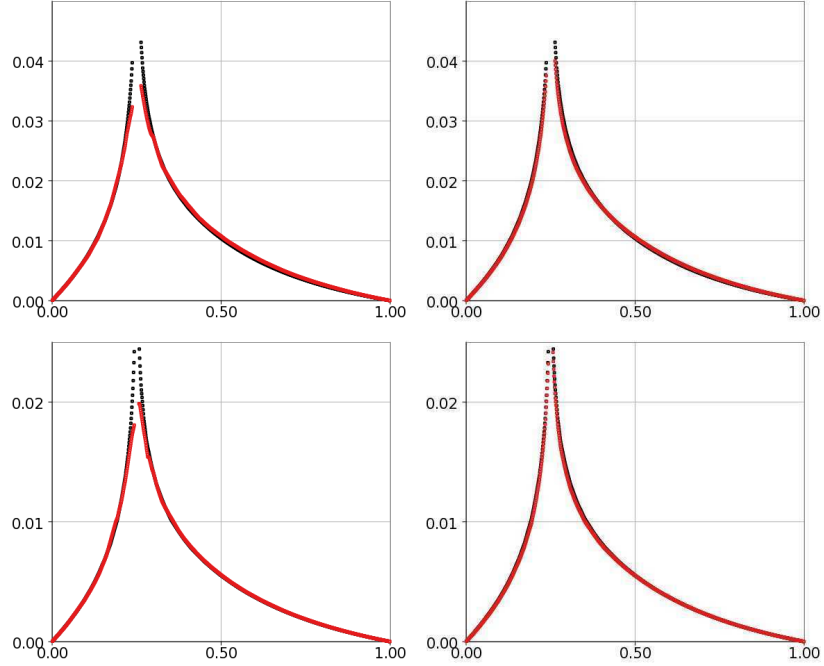
Figure 7: Profiles of the solutions a (red markers) and a_ρ (black markers) on the dashed line crossing Ω_ρ reported in Figure 6 (left). Top row: $\rho = 1.25 \cdot 10^{-2}$, $N_\rho = 629'469$. Bottom row: $\rho = 6.25 \cdot 10^{-3}$, $N_\rho = 2'393'248$. The mesh element number N for the immersed boundary computations are $N = 53'446$ in the first column, $N = 844'244$ in the second column.

refined, but the error in the H^1 norm is generally not so small as the error in the L^2 norm, because large gradients appear in the solutions near the immersed interfaces.

In particular, the smaller is the radius ρ, the more accurate is the immersed boundary solution, a. For instance, in Table 1 we see that the L^2 error reduces from 6.8% to 1.7% (in average) when the radius is halved, starting from a value corresponding to about $1/100$ of the domain diameter. We also observe that the number N of elements of the $\mathcal{T}_h^{(N)}$ mesh can be significantly smaller than that of the $\mathcal{T}_\rho^{(N_\rho)}$ mesh while providing accurate concentration profiles. For instance, from Table 1 we see that using only 97K elements (second N-column) is satisfactory, since the model error will not decrease significantly by further mesh refinement. The saving in number of mesh elements is more pronounced for small ρ, when severe mesh refinement is needed in $\mathcal{T}_{\rho,h}^{(N_\rho)}$ to represent the geometry of the thin inclusion Θ_ρ. Finally, looking at Figure 7 we notice that most of the error is concentrated near the internal boundary. More precisely, the gain in accuracy that is observed in the profiles of a using a finer mesh is

most important near Λ_s. That is why a mesh grading strategy can improve the accuracy of the immersed boundary simulations avoiding the need to refine the mesh where this is not required; this is thoroughly analyzed in [7].

5 Computational analysis of drug release from DES

Stent implantation in complex geometries such as coronary bifurcations remains a challenging problem in the clinical field. In these conditions, a lot of complications and difficulties often occur either during or after the intervention [6]. Computational analysis of such critical cases may help to improve the safety of stent implantation. Due to the limited computational cost of the proposed model, we are able to address the very challenging problem of studying drug release in stented bifurcations.

5.1 A coupled model for drug release in arteries

Before proceeding towards the discussion of numerical simulation results, we briefly summarize the entire coupled model for drug release, fluid dynamics of blood and plasma filtration and transport in the arterial lumen and wall. First of all, we split the domain representing the entire artery into two subregions, the lumen Ω_l and the wall Ω_w, denoting with a_*, b_* with $* = l, w$ the corresponding free drug concentration and density of free binding sites. More precisely, the advection-diffusion-reaction equations for drug release and transport are

$$
\begin{cases}
\partial_t a_w - \nabla \cdot (D_w \nabla a_w) + \mathbf{u}_w \cdot \nabla a_w = F_w(t, a_w) + \partial_t b_w & \text{in } \Omega_w \times \mathbb{R}^+ \\[2mm]
\partial_t b_w + k_{\text{on}} a_w b_w + k_{\text{off}} (b_w - b_{w,0}) = 0 & \text{in } \Omega_w \times \mathbb{R}^+ \\[2mm]
\partial_t a_l - \nabla \cdot (D_l \nabla a_l) + \mathbf{u}_l \cdot \nabla a_l = F_l(t, a_l) & \text{in } \Omega_l \times \mathbb{R}^+ \\[2mm]
a_l = a_w = 0 & \text{on } \Gamma_{adv} \times \mathbb{R}^+ \\[2mm]
\nabla a_l \cdot \mathbf{n}_a = \nabla a_w \cdot \mathbf{n}_a = 0 & \text{on } \Gamma_{cut} \times \mathbb{R}^+ \\[2mm]
a_l = a_{l,0}, \quad b_l = 0 & \text{in } \Omega_l \times \{t = 0\} \\[2mm]
a_w = a_{w,0}, \quad b_w = b_{w,0} & \text{in } \Omega_w \times \{t = 0\} \ .
\end{cases}
\tag{24}
$$

As discussed in [1] and confirmed by fully three dimensional computational analysis preformed in [35, 10], the interaction between mass transport and fluid dynamics is relevant to the understanding of drug deposition into the artery. The vector fields $\mathbf{u}_l$ and $\mathbf{u}_w$ in (24) represent respectively lumenal blood flow and transmural plasma filtration velocities. We model blood flow with the incompressible Navier-Stokes equations, while plasma filtration is governed by Darcy's

model. The coupled model reads as follows,

$$
\begin{cases}
\partial_t \mathbf{u}_l - \nu \Delta \mathbf{u}_l + (\mathbf{u}_l \cdot \nabla)\mathbf{u}_l + \nabla p_l = \mathbf{0} & \text{in } \Omega_l \times \mathbb{R}^+ \\[2mm]
\nabla \cdot \mathbf{u}_l = 0 & \text{in } \Omega_l \times \mathbb{R}^+ \\[2mm]
\eta \mathbf{u}_w + \nabla p_w = \mathbf{0} & \text{in } \Omega_w \times \mathbb{R}^+ \\[2mm]
\nabla \cdot \mathbf{u}_w = 0 & \text{in } \Omega_w \times \mathbb{R}^+.
\end{cases}
\tag{25}
$$

complemented with the initial, boundary and interface conditions discussed in [10].

5.2   Set up of a geometrical model for stented bifurcations

Different techniques which involve the insertion of two or more angioplastic balloons and/or stents into a coronary bifurcation are described in [23]. The preferred strategy by the physicians is the provisional side branch stenting. This technique consists of the implantation of only one stent in the main branch (MB) of the bifurcation with the opportunity of expanding another angioplastic balloon in the side branch (SB) only if the clinical results are considered suboptimal. In such a case the expansion of a balloon through the stent struts is required in order to restore the SB patency. To the best of our knowledge the effects of drug elution in a simplified model of arterial bifurcations have been investigated by means of computational models by Kolachalama et al. [24]. Their approach is not realistic as they do not include the possibility of struts that are detached from the arterial wall or stent configurations deformed nonuniformly. On the contrary, the approach here presented can be easily applied to realistic arterial stented bifurcations. Indeed, as shown in figure 2, we consider the realistic configuration of a DES implanted in a bifurcation. The stent has been represented as a one-dimensional line, according to the application of the immersed boundary method. To reach such a realistic configuration, the stented bifurcation model has been obtained running structural analyses with the method developed by Gastaldi et al. [16]. Briefly, their simulations included 7 different steps: i) positioning of the delivery system (balloon and stent) inside the coronary bifurcation; ii) expansion of the stent in the MB by means of the application of a pressure of 1 MPa on the internal surface of the balloon; iii) deflation of the MB balloon to obtain the elastic recoil of the system; iv) dilatation of the stent cell in the proximity of the bifurcation by means of the application of 1 MPa pressure on internal surface of the SB balloon; v) deflation of the SB balloon; vi) simultaneous expansion of two balloons respectively in the two branches of the bifurcation (Final Kissing Balloon) by application of a pressure 1 MPa; vii) deflation of the balloons.

5.3 Results and discussion

Combining equations (24) with the geometrical model addressed in section 5.2 and with the numerical discretization technique discussed in 4.2, we are able to perform a computational analysis of the problem.

Model (24) has to be complemented with coefficients describing drug release from a stent and mass transport in the arterial wall and lumen. We assume that the released drug is heparin, as considered in the experimental investigations presented in [25]. According to [25] we set the diffusivity of the drug in the arterial tissue to $D_w = 7.7 \times 10^{-6}$ mm^2/s and the diffusivity in the lumen to $D_w = 1.5 \times 10^{-4}$ mm^2/s. As regards the ligand/receptor interaction involving drug and proteins contributing to form the tissue extracellular matrix, i.e. equation (2), we apply the reaction constants proposed in [32], that is $k_{\mathrm{on}} = 10^2$ s^{-1} and $k_{\mathrm{off}} = 10^{-2}$ s^{-1}. The same reference provides also the average concentration of receptors in the tissue, that is set to $b_{w,0} = 5$ (we recall that all data refer to nondimensional concentrations). To completely close problem (24) we assume the at the initial time the artery does not contain drug, namely $a_{w,0} = a_{l,0} = 0$. For the stent coating, we estimate a thickness $L = 7$ μm and we assume that the initial drug charge is $s_0 = 10$. The diffusivity of the drug within the coating strongly depends on the material that has been chosen for this purpose. Most often, DES are coated with polymers, in particular aliphatic polyesters such as poly-lactic or poly-glycolic acids. Furthermore, the parameter D_c also depends on the average polymeric chain length and density of such materials [33]. A reasonable average value seems to be $D_c = 10^{-8}$ mm^2/s, also confirmed by [32]. Such data, together with equation (15) allows us to find a preliminary estimate of the emptying time of the stent. In particular, setting $a = 0$ in (15) we obtain that after $T = 6$h 20$'$ about 95% of the available drug has been released.

The most significant feature of concentration profiles reported in figure 8 consists in the fact that the highest concentrations are located on the opposite part of the artery with respect to the bifurcation branch. Such effect can be explained by a combination of fluid dynamics and mass transport phenomena. The origin of these profiles resides in a specific feature of the artery configuration after the implantation of a stent with the kissing-balloon technique (see Section 5.2). As a consequence of such a technique, the deformation of the artery deviates from the original axial-symmetric configuration and the cross section of the artery assumes an elliptic shape, more elongated on the plane that contains the bifurcation branch. Figure 9 confirms that such configuration is responsible for promoting low axial velocities and possible blood recirculations on the lower part of the lumen, combined with the fact that the bifurcation subtracts a considerable part of the flow from the upper part of the artery (where top and bottom refer to the orientation of pictures in figure 8). As already observed in [1] for the case of DES and in [30] for the study of atherosclerosis, penetration of chemicals is promoted into regions of low axial blood flow, because the components of the transversal velocities towards the arterial wall are more relevant.
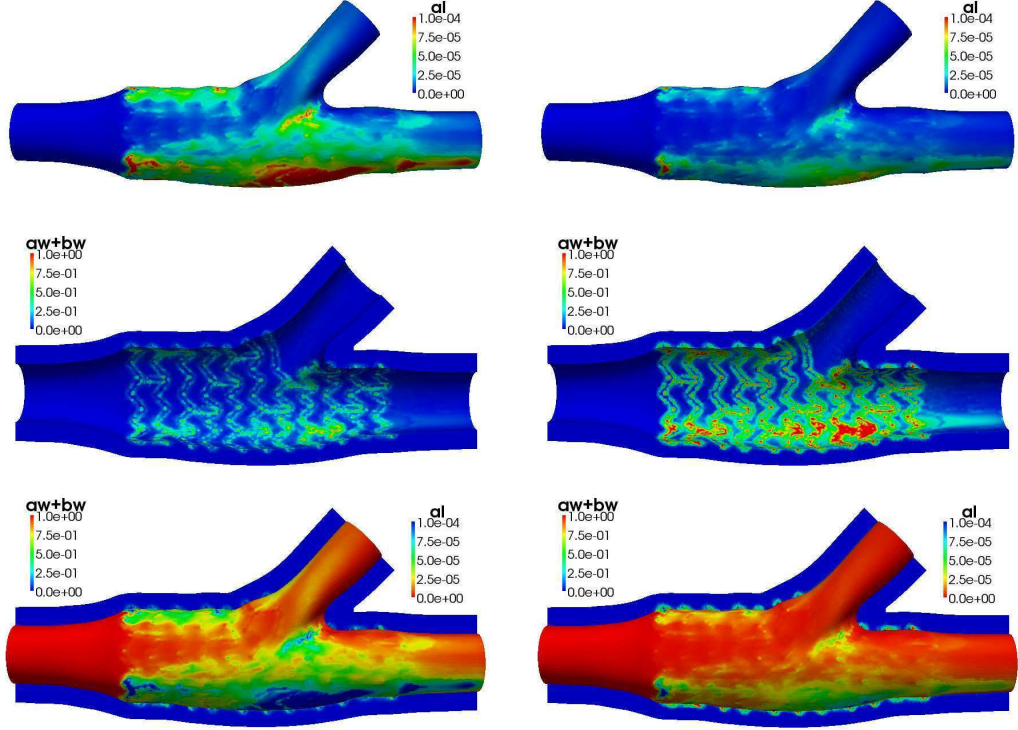
Figure 8: Concentration profiles in the artery a_l, $a_w + d_w$, $a_l + a_w + d_w$ from top to bottom, at different times $t = 30'$, $t = 5$ h from left to right.

A second significant remark consists in the analysis of the drug distribution into the arterial wall for relatively long time periods, see figure 8 with $t = 5$ h. Indeed, we observe that the drug does not uniformly distribute in the wall, but the concentration of the drug is much higher in the neighborhood of the stent filaments. This is due to the ligand/receptor interaction between the drug and the tissue where the forward reaction in (2), characterized by constant $k_{\text{on}} = 10^2$ s^{-1}, is much faster than the backward one, driven by $k_{\text{off}} = 10^{-2}$ s^{-1}. As a result of that, the drug in the arterial wall is mostly present in the bound state, denoted by d_w, which can neither diffuse nor be transported by the slow filtration of plasma across the wall.

Finally, we validate the results of section 3 by means of a comparison with the full three-dimensional simulations of model (24). The most important quantity to analyze is the evolution in time of the free drug concentration in the lumen and in the wall, namely a_l and a_w, in order to verify whether assumption 3.1 is satisfactorily verified or not. We denote by $\bar{a}_*(s, t)$, $* = l, w$, the mean value along each virtual perimeter, $\gamma(s)$, of the immersed boundary model of the stent
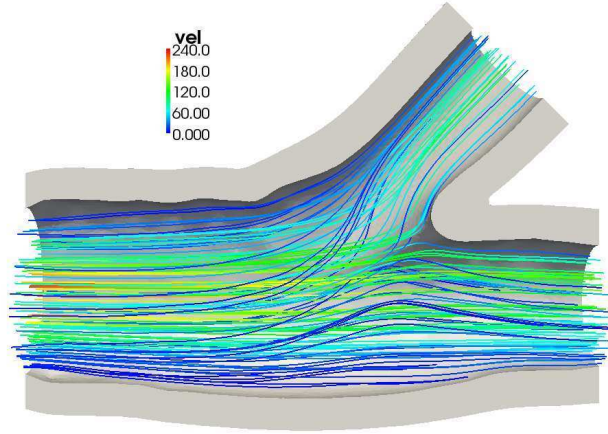
Figure 9: Streamlines of blood flow in the lumen. Colors denote the velocity magnitude in cm/s.

(see figure 5)

$$\bar{a}_*(s,t) := \frac{1}{\xi_*(s)|\gamma(s)|} \int_{\gamma(s)} a_*(\mathbf{x},t)\xi_*(s)\,d\mathbf{x}\,.$$

We then consider the maximal value along the arc length of $\bar{a}_*(s,t)$, more precisely $\bar{\bar{a}}_*(t) := \max_{s \in \Lambda_s} |\bar{a}_*(s,t)|$.
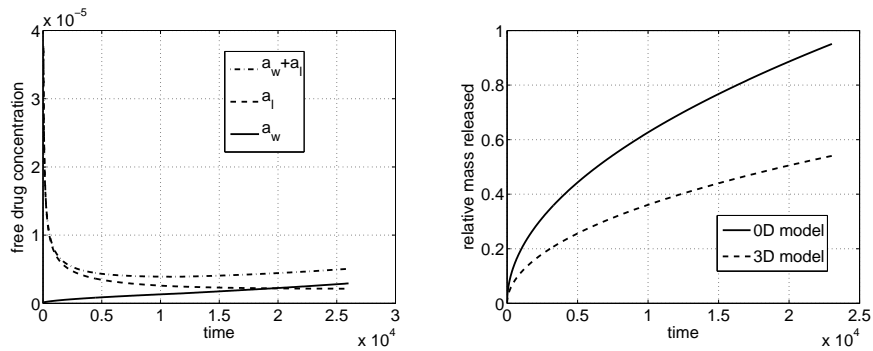

Figure 10: The evolution of the concentrations $\bar{\bar{a}}_l(t)$, $\bar{\bar{a}}_w(t)$ and $\bar{\bar{a}}_l(t) + \bar{\bar{a}}_w(t)$ with time (left). A comparison of the relative amount of released drug (right) estimated by model (24) (label 3D) and by model (15) (label 0D).

Figure 10 (left) shows that the requirements of assumption 3.1 are accurately satisfied. On the one hand, the small variations of the concentration in the lumen, a_l, are justified reminding us that the governing equation for drug released

24

in the lumen consists of a transport dominated advection diffusion equation. As a result of that the drug released by the surface of the stent exposed to blood flow is immediately washed away. Possible effects of drug accumulation in the fluid recirculation in proximity of the stent cannot be taken into account here, because the immersed boundary model of the stent does not affect the blood stream. Anyway, for a realistic three-dimensional stent model, it was shown in [35] that these phenomena minimally affect drug release. On the other hand, a_w is small because of the previously mentioned ligand/receptor reaction.

In a second test, we analyze the relative amount of drug released. For the three-dimensional model, this quantity is defined as $q(t)/q_\infty|_{3D}$ where $q_\infty|_{3D} = s_0 L|\Gamma_s|$ while $q(t)|_{3D}$ is

$$q(t)|_{3D} = \int_{\Omega_w} \big(a_w(\mathbf{x},t) + d_w(\mathbf{x},t)\big)\, d\mathbf{x} + \int_{\Omega_l} a_l(\mathbf{x},t)\, d\mathbf{x}.$$

Concerning the amount of released drug estimated by (15), we proceed as in the comparison with Higuchi's model, with the difference that now the external concentration is the function $\bar{\bar{a}}_l(t) + \bar{\bar{a}}_w(t)$ computed with model (24). The fact that the estimate relative to the fully three-dimensional model is considerably lower than the one for the lumped model, as depicted in figure 10 (right), indicates that part of the total drug release is removed from the vascular district under consideration. This can be explained by noticing that most of the drug released in the lumen is transported away. Furthermore, also part of the drug penetrating in the arterial wall can abandon the arterial tissue, because of the possible exchange of drug between lumen and wall. The former source of loss is predominant, as confirmed by observing that the amount of drug penetrating into the arterial wall is approximately half the total, in agreement with the fact that half of the stent surface is exposed to blood flow.

Conclusions

We have shown that the present multiscale model for drug release, complemented with the mechanical analysis of stent expansion, see for instance [27, 35, 16], represents a complete tool to study mechanics, fluid dynamics and pharmacokinetics of realistic and complex cases of DES implantation, with affordable computational cost on any up to date computing platform. We hope that in silico analyses may become in future a complementary tool for DES design and clinical investigation.

References

[1] B. BALAKRISHNAN, A.R. TZAFRIRI, P. SEIFERT, A. GROOTHUIS, C. ROGERS, AND E.R. EDELMAN. *Strut position, blood flow, and drug*

deposition. Implications for single and overlapping drug-eluting stents. Circulation, 111 (2005), pp. 2958–2965.

[2] P.BISCARI, S.MINISINI, D.PIEROTTI, G.VERZINI, P.ZUNINO. *Controlled release with finite dissolution rate*, *SIAM J. Appl. Math.*, 71 (2011), pp. 731–752.

[3] E.BURMAN, P.HANSBO. *Edge stabilization for Galerkin approximations of convection-diffusion-reaction problems.* Comput. Methods Appl. Mech. Engrg., 193 (2004), pp. 1437–1453.

[4] E. BURMAN AND P. ZUNINO. *A domain decomposition method based on weighted interior penalties for advection-diffusion-reaction problems. SIAM J. Numer. Anal.*, 44 (2006), pp. 1612–1638.

[5] D.S. COHEN AND T. ERNEUX. *Controlled Drug Release Asymptotics*, SIAM J. Appl. Math., 58 (1998), pp. 1193–1204.

[6] A.COLOMBO, JW MOSES, MC MORICE, J LUDWIG, DR HOLMES JR, V SPANOS, Y LOUVARD, B DESMEDT, C DI MARIO, MB LEON. *Randomized study to evaluate sirolimus-eluting stents implanted at coronary bifurcation lesions.* Circulation, 109 (2004) pp. 1244–1253.

[7] C. D'ANGELO. *Finite Element Approximation of Elliptic Problems with Dirac Measure Terms in Weighted Spaces. Applications to 1D-3D Coupled Problems.* MOX Report 39/2010, submitted, 2010.

[8] C. D'ANGELO AND A. QUARTERONI. *On the coupling of 1D and 3D diffusion-reaction equations. Application to tissue perfusion problems.* Math. Models Methods Appl. Sci., 18 (2008) pp. 1481–1504.

[9] C. D'ANGELO AND P. ZUNINO. *Multiscale models of drug delivery by thin implantable devices.* In Applied and industrial mathematics in Italy III, Ser. Adv. Math. Appl. Sci., 82 (2009), pp. 298–310.

[10] C. D'ANGELO AND P. ZUNINO. *Robust numerical approximation of coupled Stokes' and Darcy's flows applied to vascular hemodynamics and biochemical transport.* ESAIM: M2AN, 45 (2011), pp. 447–476.

[11] P. DEUFLHARD. *A modified Newton method for the solution of ill-conditioned systems of nonlinear equations with application to multiple shooting.* Numer. Math., 22 (1974), pp. 289–315.

[12] R. FATTORI, T. PIVA. *Drug-eluting stents in vascular intervention.* Lancet., 361 (2003), pp. 247–249.

[13] L. FORMAGGIA, S. MINISINI, AND P. ZUNINO. *Modeling erosion controlled drug release and transport phenomena in the arterial tissue.* Math. Mod. Meth. Appl. Sci., (M3AS), 20 (2010), pp. 1759–1786.

[14] G. Frenning. *Theoretical investigation of drug release from planar matrix systems: effects of a finite dissolution rate.* J. Control. Release, 92 (2003), pp. 331–339.

[15] G. Frenning. *Theoretical analysis of the release of slowly dissolving drugs from spherical matrix systems.* J. Control. Release, 95 (2004) pp. 109–117.

[16] D. Gastaldi, S. Morlacchi, R. Nichetti, C. Capelli, G. Dubini, L. Petrini, F. Migliavacca. *Modelling of the provisional side-branch stenting approach for the treatment of atherosclerotic coronary bifurcations: effects of stent positioning.* Biomech. Model. Mechanobiol., 9 (2010), pp. 551–561.

[17] E. Hairer and G. Wanner. *Solving ordinary differential equations II*, Springer Series in Computational Mathematics 14, Springer-Verlag, Berlin, 2nd ed., 1996.

[18] T. Higuchi. *Rate of release of medicaments from ointment bases containing drugs in suspension*, J. Pharmac. Sci., 50 (1961), pp. 874–875.

[19] T. Higuchi. *Mechanism of sustained-action medication—Theoretical analysis of rate of release of solid drugs dispersed in solid matrices.* J. Pharmac. Sci., 52 (1963), pp. 1145–1149.

[20] B.L. van der Hoeven, N.M. Pires, H.M. Warda, P.V. Oemrawsingh, B.J. van Vlijmen, P.H. Quax, M.J. Schalij, E.E. van der Wall and J.W. Jukema. *Drug-eluting stents: results, promises and problems.* International Journal of Cardiology,99 (2005), pp. 9–17.

[21] C.W. Hwang, D. Wu, and E.R. Edelman. *Physiological transport forces govern drug distribution for stent-based delivery.* Circulation, 104 (2001), pp. 600–605.

[22] D.R. Hose, A.J. Narracott, B. Griffiths, S. Mahmood, J. Gunn, D. Sweeney and P. Lawford. *A thermal analogy for modelling drug elution from cardiovascular stents.* Computer Methods in Biomechanics and Biomedical Engineering, 7 (2004), pp. 257–264.

[23] I. Iakovou and A. Colombo. *Contemporary stent treatment of coronary bifurcations.* J Am Coll Cardiol., 46 (2005), pp. 1446–1455.

[24] V.B. Kolachalama, E.G. Levine, E.R. Edelman. *Luminal flow amplifies stent-based drug deposition in arterial bifurcations.* PLoS One, 4 (2009) e8105.

[25] M.A. Lovich and E.R. Edelman, *Computational simulations of local vascular heparin deposition and distribution*, Am. J. Physiol., 271 (1996), pp. 214–224.

[26] P. Macheras and A. Iliadis. *Modeling in biopharmaceutics, pharmacokinetics, and pharmacodynamics*, Interdisciplinary Applied Mathematics, 30, Springer, New York, 2006.

[27] F. Migliavacca, F. Gervaso, M. Prosi, P. Zunino, S. Minisini, L. Formaggia and G. Dubini. *Expansion and drug elution model of a coronary stent.* Computer Methods in Biomechanics and Biomedical Engineering, 10 (2007), pp. 63–73.

[28] C.S. Peskin. *Flow patterns around heart valves.* In Proceedings of the Third International Conference on Numerical Methods in Fluid Mechanics (Univ. Paris VI and YI, Paris, 1972), Vol. II, pages 214–221. Lecture Notes in Phys., Vol. 19, Berlin, 1973. Springer.

[29] C.S. Peskin. *The fluid dynamics of heart valves: experimental, theoretical, and computational methods.* In Annual review of fluid mechanics, 14 (1982), pp. 235–259. Annual Reviews, Palo Alto, Calif.

[30] M. Prosi, P. Zunino, K. Perktold, and A. Quarteroni, *Mathematical and numerical models for transfer of low-density lipoproteins through the arterial walls: A new methodology for the model set up with applications to the study of disturbed lumenal flow*, J. Biomech., 38 (2005), pp. 903–917.

[31] A. Quarteroni and A. Valli. *Numerical approximation of partial differential equations*, Springer Series in Computational Mathematics, 23, Springer-Verlag, Berlin, 1994.

[32] D.V. Sakharov, L.V. Kalachev and D.C. Rijken, *Numerical simulation of local pharmacokinetics of a drug after intravascular delivery with an eluting stent*, J. Drug Targ., 10 (2002), pp. 507–513.

[33] J.S. Soares, P. Zunino. *A mixture model for water uptake, degradation, erosion, and drug release from polydisperse polymeric networks.* Biomaterials, 31 (2010), pp. 3032–3042.

[34] C. Vergara and P. Zunino. *Multiscale boundary conditions for drug release from cardiovascular stents*, Multiscale Model. Simul., 7 (2008), pp. 565–588.

[35] P. Zunino, C. D'Angelo, L. Petrini, C. Vergara, C. Capelli, and F. Migliavacca. *Numerical simulation of drug eluting coronary stents: mechanics, fluid dynamics and drug release*, Comput. Meth. Appl. Mech. Eng., 198 (2009), pp. 3633–3644.

[36] P. Zunino. *Multidimensional pharmacokinetic models applied to the design of drug-eluting stents.* International Journal of Cardiovascular Engineering, 4 (2004), pp. 181–191.

MOX Technical Reports, last issues

Dipartimento di Matematica "F. Brioschi",
Politecnico di Milano, Via Bonardi 9 - 20133 Milano (Italy)

40/2011 D Angelo, C.; Zunino, P.; Porpora, A.; Morlacchi, S.; Migliavacca, F.
Model reduction strategies enable computational analysis of controlled drug release from cardiovascular stents

39/2011 Antonietti, P.F.; Ayuso de Dios, B.; Brenner, S.C.; Sung, L.-Y.
Schwarz methods for a preconditioned WOPSIP method for elliptic problems

38/2011 Porpora A., Zunino P., Vergara C., Piccinelli M.
Numerical treatment of boundary conditions to replace lateral branches in haemodynamics

37/2011 Ieva, F.; Paganoni, A.M.
Depth Measures For Multivariate Functional Data

36/2011 Motamed, M.; Nobile, F.; Tempone, R.
A stochastic collocation method for the second order wave equation with a discontinuous random speed

35/2011 Iapichino, L.; Quarteroni, A.; Rozza, G.
A Reduced Basis Hybrid Method for the coupling of parametrized domains represented by fluidic networks

34/2011 Benacchio, T.; Bonaventura, L.
A spectral collocation method for the one dimensional shallow water equations on semi-infinite domains

33/2011 Antonietti, P.F.; Beirao da Veiga, L.; Lovadina, C.; Verani, M.
Hierarchical a posteriori error estimators for the mimetic discretization of elliptic problems

32/2011 Aletti, G; Ghiglietti, A; Paganoni, A.
A modified randomly reinforced urn design

31/2011 Astorino, M.; Becerra Sagredo, J.; Quarteroni, A.
A modular lattice Boltzmann solver for GPU computing processors